Immuno-PET Imaging of CD30-Positive Lymphoma Using ^{89}Zr-Desferrioxamine–Labeled CD30-Specific AC-10 Antibody

Svetlana N. Rylova[1–3], Luigi Del Pozzo[1–3], Cathrin Klingeberg[1,3,4], Roswitha Tönnesmann[2], Anna L. Illert[1,3,4], Philipp T. Meyer[1,2], Helmut R. Maecke[2], and Jason P. Holland[1–3]

[1]German Cancer Consortium, Heidelberg, Germany; [2]Department of Nuclear Medicine, University Hospital Freiburg, Freiburg, Germany; [3]German Cancer Research Center, Heidelberg, Germany; and [4]Department of Internal Medicine I, University Hospital Freiburg, Freiburg, Germany

The CD30-specific antibody–drug conjugate, brentuximab vedotin, is approved for the treatment of relapsed, refractory Hodgkin lymphomas and systemic anaplastic large T-cell lymphomas. Multiple ongoing clinical trials are investigating brentuximab vedotin efficacy in other CD30-positive hematologic malignancies. Because CD30 expression varies among different types of lymphoma and can also change during the course of treatment, companion diagnostic imaging of CD30 could be a valuable tool in optimizing patient-specific brentuximab vedotin treatment regimens. **Methods:** The mouse antihuman CD30 antibody AC-10 was radiolabeled with the positron-emitting radionuclide ^{89}Zr. The stability and specificity of ^{89}Zr-desferrioxamine (DFO)-labeled CD30-specific AC-10 antibody (^{89}Zr-DFO-AC-10) was evaluated in vitro. The pharmacokinetics of ^{89}Zr-DFO-AC-10 was studied in BALB/c nude mice bearing subcutaneous human Karpas 299 tumors (CD30-positive model) or A-431 tumors (CD30-negative model) using PET/CT imaging, biodistribution studies, and autoradiography. **Results:** AC-10 was conjugated with a DFO B chelator and radiolabeled with ^{89}Zr to give formulated ^{89}Zr-DFO-AC-10 with a radiochemical yield of 80%, radiochemical purity greater than 99%, and specific activity of 111–148 MBq/mg. ^{89}Zr-DFO-AC-10 was stable in mouse and human sera and preserved the immunoreactivity toward CD30. Biodistribution data showed the highest tissue accumulation of ^{89}Zr-DFO-AC-10 in CD30-positive tumors, with 37.9% ± 8.2% injected activity per gram of tissue at 72 h after injection, whereas uptake in CD30-negative tumors was 11.0% ± 0.4%. The specificity of ^{89}Zr-DFO-AC-10 binding to CD30 in vivo was confirmed by blocking studies. Time–activity curves showed that between 24 and 144 h after injection, tumor-to-muscle ratios increased from 18.9 to 51.8 in the CD30-positive model and from 4.8 to 8.7 in the CD30-negative model. Tumor-to-blood ratios also increased, from 3.2 to 13.6 and from 1 to 2 in the CD30-positive and -negative models, respectively. **Conclusion:** Our results demonstrate that for measuring CD30 expression, ^{89}Zr-DFO-AC-10 is a sensitive PET agent with high tumor–to–normal-tissue contrast. ^{89}Zr-DFO-AC-10 is a promising CD30-imaging radiotracer for clinical translation in patients with various lymphomas and other diseases.

CD30, a member of the tumor necrosis factor superfamily, is expressed by Reed–Sternberg cells and used as a primary diagnostic marker for Hodgkin lymphoma (1). CD30 is also highly expressed on the surface of some T-cell lymphomas, especially on anaplastic large cell lymphoma, and at variable levels on a subset of other non-Hodgkin lymphomas, including diffuse large B-cell lymphoma (2–4). Expression of CD30 in healthy tissues is restricted to activated T and B cells, and the receptor cannot be found outside the immune system (2,5). High expression levels on specific cancers and limited presentation in healthy tissues make CD30 an ideal target for antibody-based molecular therapies.

Brentuximab vedotin (Adcentris; Seattle Genetics), an antibody–drug conjugate consisting of a CD30-specific antibody conjugated to the antimitotic agent monomethyl auristatin E, was approved by the U.S. Food and Drug Administration for treatment of patients with relapsed or refractory CD30-positive Hodgkin lymphoma and anaplastic large cell lymphoma (6,7). In 2 phase II trials, brentuximab vedotin showed an impressive clinical response, with respective objective and complete response rates of 75% and 34% in Hodgkin lymphoma and 86% and 59% in anaplastic large cell lymphoma (8–10). A recent phase III study in Hodgkin lymphoma demonstrated median progression-free survival of 43 mo for patients treated with brentuximab vedotin versus 24 mo for those receiving placebo (11,12). Importantly, another phase II clinical trial proved the efficacy of brentuximab vedotin in CD30-positive non-Hodgkin lymphoma with lower CD30 expression levels. The objective response rate in CD30-positive diffuse large B-cell lymphoma was 44% (13). Moreover, this study concluded that brentuximab vedotin can be combined safely with rituximab for simultaneous treatment of CD20-positive lymphomas. On the basis of clinical experience, brentuximab vedotin offers a promising alternative treatment option for refractory Hodgkin lymphomas and non-Hodgkin lymphomas that relapse or do not respond to the standard chemotherapy regimens.

Despite the growing clinical use of brentuximab vedotin, there is no companion diagnostic imaging tool available for selecting patients and predicting or monitoring response to CD30-targeted chemotherapy. Clinical studies have also highlighted the lack of precise quantification methods to estimate CD30 expression in lymphomas as a current

impediment to optimum patient management (*11–14*). At present, it remains unclear whether there exists a threshold level of CD30-positive lymphoma cells that is required for effective brentuximab vedotin treatment. The bystander effect caused by a diffusible monomethyl auristatin E component has been identified as an important mechanism of brentuximab vedotin efficacy in tumors with low CD30 expression. Identification of precise CD30 expression in vivo by PET imaging gives the opportunity to answer outstanding clinical questions associated with CD30 expression and brentuximab vedotin treatment efficacy. Moreover, the use of a CD30-specific PET tracer may help optimize brentuximab vedotin dose regimens and detect minimal residual lymphoma with a high risk of relapse.

To our knowledge, there is only one report describing fluorescent imaging with CD30-specific single-strand DNA–based aptamer probes (*15*), and one abstract describing the use of radiolabeled brentuximab vedotin for PET imaging of CD30 protein expression in human xenografts (*16*). However, imaging with radiolabeled antibody–drug conjugates is suboptimal in the clinical setting because of concerns about toxicity. Here, we report preclinical PET imaging of CD30-positive human lymphomas in a mouse model using ^{89}Zr-desferrioxamine (DFO)-labeled CD30-specific AC-10 antibody (^{89}Zr-DFO-AC-10), which has the same affinity and target specificity as the native antibody component of brentuximab vedotin.

MATERIALS AND METHODS

Full details on all methods and equipment are presented in the supplemental materials (available at http://jnm.snmjournals.org).

Antibody Expression and Conjugation

The IgG$_{2b}$ murine monoclonal antibody (mAb) AC-10 was expressed from an AC-10 hybridoma (a gift from Prof. Eckhard Podack, University of Miami) and purified using protein G Sepharose (GE Healthcare) in accordance with standard protocols. Purified AC-10 was conjugated to *p*-isothiocyanatobenzyl-DFO B (MacrocyclicsX) using the methods of Vosjan et al. (*17*) with slight modifications. The antibody-to-DFO ratio was 1:5, and the reaction was performed at pH 9.5. Protein concentrations were measured using the bicinchoninic acid method (Pierce; Thermo Fisher Scientific Inc.).

Radiolabeling

^{89}Zr-oxalate in 1 M oxalic acid was purchased from Perkin Elmer. The specific activity was measured using a modified method adapted from previous reports (*18*). The DFO-AC-10 conjugated antibody was radiolabeled using standard procedures (*17,19–21*). The radiochemical yield and radiochemical purity were determined using radio–thin-layer chromatography or radio–high-performance liquid chromatography equipped with an ENrich size-exclusion column (Bio-Rad Laboratories GmbH).

The number of accessible chelators on DFO-AC-10 was determined experimentally by radiolabeling the conjugated mAb with excess ^{89}Zr-oxalate. The moles of zirconium bound (calculated using the measured specific activity of the ^{89}Zr stock) and the protein concentrations were used to calculate the ratio of the number of accessible chelators per antibody.

Fluorescence-Activated Cell Sorting and Cellular Binding Assays In Vitro

The cells (1×10^6) were washed with phosphate-buffered saline (PBS), blocked in flow cytometry staining buffer (eBioscience,) and incubated with AC-10 antibodies or IgG$_{2b}$ isotype control (Sigma) at a 1 μg/mL concentration in blocking buffer at 4°C for 30 min. Subsequently, the cells were incubated with goat antimouse secondary antibody (Life Technologies GmbH) conjugated to phycoerythrin. Cell-bound fluorescence was measured using a CyAn ADP flow cytometer (Beckman Coulter), and data were analyzed using FlowJo software (FlowJo).

For in vitro cell-binding assays, serial dilutions of cells (in the range of 1×10^5 to 2.5×10^6 cells) in triplicate were incubated with ^{89}Zr-DFO-AC-10 (~6.8 kBq [~0.18 μCi]; 45–60 ng of protein) in PBS containing 1% bovine serum albumin at room temperature for 1 h on an orbital shaker. After 2 washings with PBS, cell-bound radioactivity was measured using a γ-counter (Cobra 5003; Packard Instruments). The percentage of specifically bound ^{89}Zr activity was assessed by comparison with standards and controls.

Serum Stability

The stability of ^{89}Zr-DFO-AC-10 with respect to change in radiochemical purity via loss of radioactivity from the mAb was investigated in vitro by incubation in solutions of human or mouse serum (Sigma Aldrich) at 37°C. The radiochemical purity was determined by radio–high-performance liquid chromatography on an ENrich size-exclusion column with a PBS/diethylenetriaminepentaacetic acid (1 mM) mobile phase at a flow rate of 1.25 mL/min.

Xenograft Models

All animal experiments were conducted according to the regulations of the University Medical Center of Freiburg. Female BALB/c nude mice (18–20 g, 6–8 wk old) were obtained from Janvier Labs. In separate animals, Karpas 299 CD30-positive and A-431 CD30-negative tumors were induced on the right shoulder by subcutaneous injection of 20–25 million Karpas 299 cells in a 1:1 v/v mixture of PBS and Matrigel (Corning) or 5 million A-431 cells in PBS (final volume, 100 μL).

Biodistribution Studies

Karpas 299 and A-431 tumor-bearing mice were randomized before the study and were warmed gently with a heat lamp before ^{89}Zr-DFO-AC-10 was administered via tail-vein injection (0.55–0.74 MBq, 8 μg of mAb in 100-μL sterile saline for injection; t = 0 h). Animals (n = 3–4, per group) were euthanized by asphyxiation with excess isoflurane at 24, 72, and 144 h after radiotracer administration, and 12 tissues (including the tumor) were removed, rinsed in water, dried in air, weighed, and counted on a calibrated and normalized γ-counter for accumulation of ^{89}Zr-radioactivity.

Digital Autoradiography and Histology

Tumors were fast-frozen on dry ice, embedded in optimal-cutting-temperature compound, and cut into 10-μm sections using a CM1950 cryomicrotome (Leica). Sections were exposed on a Super Resolution phosphor screen (Perkin Elmer) for 14 h. The digital autoradiography images were obtained by scanning the phosphor screens on a Cyclone Plus phosphor imager (Perkin Elmer). Adjacent 10-μm slices were stained with hematoxylin–eosin and scanned using Panoramic SCAN 150 (3D Histech).

Small-Animal PET/CT Imaging

PET imaging was conducted on a microPET Focus 120 scanner (Concorde Microsystems) (*22*). The mice were administered ^{89}Zr-DFO-AC-10 (6.9–7.5 MBq, 80–82 μg of mAb in 100 μL of sterile saline) via tail-vein injection. Full details are presented in the supplemental materials.

Statistical Analysis

Statistical analyses were performed using Prism, version 5.01 (GraphPad Software, Inc), and Excel (Microsoft). Data were analyzed using the unpaired, 2-tailed Student t test. Differences at the 95% confidence level ($P < 0.05$) were considered to be statistically significant.

RESULTS

Antibody Expression, DFO Conjugation, and Flow Cytometry

The murine monoclonal IgG$_{2b}$ antihuman CD30 antibody (clone AC-10) was expressed using an AC-10 hybridoma (Supplemental Fig. 1). After isolation, the AC-10 antibody was conjugated to
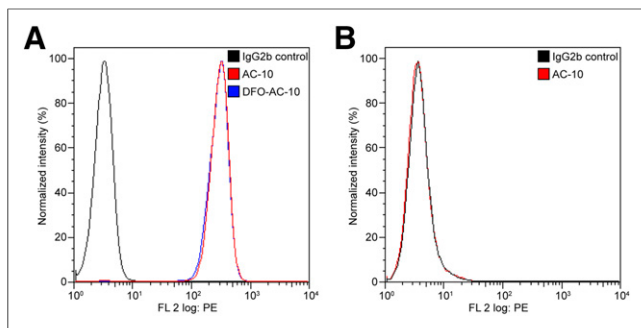
FIGURE 1. (A) Flow cytometry data showing specific binding of AC-10 and DFO-AC-10 to CD30-positive Karpas 299 cells. (B) Control data showing that AC-10 antibody does not bind to CD30-negative A-431 cells. FL = ···; PE = phycoerythrin.

p-isothiocyanato-benzyl-DFO B and the resulting conjugate was purified via standard procedures to give DFO-AC-10 (*17*). Flow cytometry was then used to assess the binding of AC-10 and DFO-AC-10 antibody to CD30-positive Karpas 299 cells (Fig. 1A). The fluorescence-activated cell-sorting data showed that both AC-10 and DFO-AC-10 antibodies bound to Karpas 299 cells. The mean fluorescence intensity was 327 and 316 for AC-10 and DFO-AC-10, respectively. Mean fluorescence intensity was only 3 in IgG$_{2b}$ control samples. In contrast to studies on CD30-positive cells, the AC-10 antibody did not bind to A-431 CD30-negative cells, and the mean fluorescence intensity was the same as in the negative control stained with IgG$_{2b}$ (Fig. 1B). These fluorescence-activated cell-sorting data provided confidence in using DFO-AC-10 for further radiolabeling studies.

Radiochemistry and Serum Stability

DFO-AC-10 was radiolabeled with ^{89}Zr-oxalate to give ^{89}Zr-DFO-AC-10 in accordance with previously reported procedures (*19,21*). After purification by size-exclusion chromatography (PD-10 columns or spin-column centrifugation), ^{89}Zr-DFO-AC-10 was formulated in sterile saline for injection with a radiochemical purity of more than 99%, an average radiochemical yield of about 80% (*n* = 5), and an effective specific activity of 111–148 MBq/mg (3–4 mCi/mg) of protein. The number of accessible chelators per antibody was measured from saturation labeling experiments to be 5.1 ± 0.3. These data also indicate that the DFO conjugation reaction proceeded quantitatively.

During the quality control we noted that ^{89}Zr-DFO-AC-10 displayed a propensity toward aggregation after purification had been performed using PD-10 size-exclusion chromatography with saline as an eluent. Protein aggregation was circumvented using size-exclusion

spin-column centrifugation (Fig. 2A) with approximately only 3% aggregates identified in the final formulated solution of ^{89}Zr-DFO-AC-10. Stability studies revealed that ^{89}Zr-DFO-AC-10 showed no change in radiochemical purity with regard to protein aggregation or loss of ^{89}Zr activity from the mAb fraction over time (Figs. 2B and 2C, respectively).

Cellular Binding

To confirm that the conjugation and ^{89}Zr-radiolabeling chemistry did not compromise antibody immunoreactivity, cellular binding assays were performed (Fig. 3). The data revealed that as the number of CD30-positive Karpas 299 cells increased (in the range of 1×10^5 to 2.5×10^6 cells per well), ^{89}Zr-DFO-AC-10 binding also increased to more than 98% specifically bound activity. Control experiments using CD30-negative A-431 cells showed no specific binding (Fig. 3). Collectively, these data confirmed that ^{89}Zr-DFO-AC-10 retained high immunoreactivity and specificity for CD30.

Biodistribution Data

Ex vivo biodistribution studies conducted at 24 and 72 h after administration of ^{89}Zr-DFO-AC-10 in separate groups of Karpas 299 and A-431 tumor-bearing mice found that the radiotracer displays a background distribution and tumor uptake similar to other reported ^{89}Zr-DFO-mAb radiotracers (Table 1; Fig. 4). Tumor uptake in the CD30-positive Karpas 299 model was 27.2 ± 6.0 percentage injected activity (%IA)/g at 24 h, and this uptake continued to increase to 37.9 ± 8.2 %IA/g by 72 h after administration. In contrast, accumulation of radioactivity in the A-431 CD30-negative model was significantly lower, reaching only 8.2 ± 1.6 and 11.0 ± 0.4 %IA/g at 24 and 72 h, respectively, after administration ($P <$ 0.01 for comparisons between tumor models at the respective time points). The highest accumulation of ^{89}Zr radioactivity among normal organs was in the liver, with 15.22 ± 1.71 %IA/g at 24 h after injection and 11.78 ± 2.43 %IA/g at 72 h after injection in Karpas 299 tumor-bearing mice. At 72 h after radiotracer administration, liver uptake of ^{89}Zr radioactivity in the CD30-negative model was the same as in the positive model (12.61 ± 2.20 %IA/g).

Among the normal tissues, blood-pool activity differed significantly between models. At both the 24- and the 72-h time points, radioactivity in the blood of A-431 tumor-bearing animals remained higher (15.8 ± 2.3 and 12.2 ± 2.2 %IA/g, respectively) than in the corresponding groups of mice bearing Karpas 299 tumors (9.9 ± 2.7 and 6.4 ± 0.5 %IA/g, respectively). These data are consistent with the extraction of activity from the blood pool into the CD30-positive tumors and support the conclusions that the ^{89}Zr-DFO-AC-10 retains high immunoreactivity in vivo and that the tumor uptake is specific.

Further demonstration of CD30-targeting specificity was obtained from blocking studies using biodistribution in Karpas 299 tumor-bearing mice (Table 1; Fig. 4). Tumor accumulation of ^{89}Zr radioactivity in the blocking group at 72 h after injection was 22.5 ± 1.6 %IA/g ($P <$ 0.05 for comparison with the nonblocking group), whereas blood-pool activity remained higher, at 9.5 ± 2.6 %IA/g. Hence, blocking induced an approximately 40% decrease in tumor uptake. These data confirm the specific targeting of CD30 by ^{89}Zr-DFO-AC-10 in vivo.
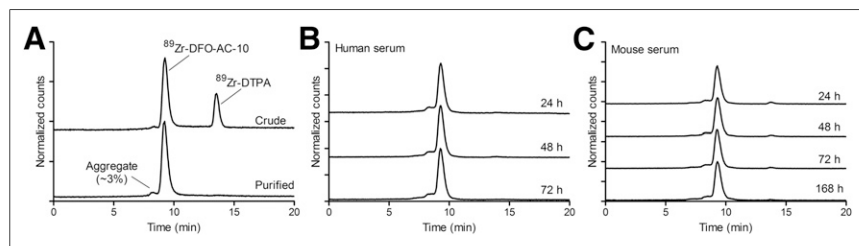
FIGURE 2. (A) Size-exclusion radio–high-performance liquid chromatograms showing radiochemical purity of formulated sample of ^{89}Zr-DFO-AC-10. (B and C) Size-exclusion radio–high-performance liquid chromatogram data showing radiochemical stability of ^{89}Zr-DFO-AC-10 after incubation at 37°C in human and mouse sera. DTPA = diethylenetriaminepentaacetic acid.
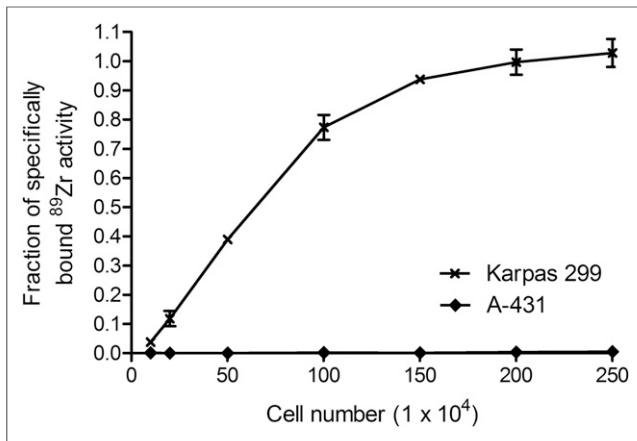
FIGURE 3. Cellular uptake data showing saturation of specific binding of ^{89}Zr-DFO-AC-10 to CD30-positive Karpas 299 cells and lack of binding to CD30-negative A-431 cells.

PET/CT Imaging

Temporal PET/CT imaging was performed on groups of 3 mice bearing either Karpas 299 or A-431 tumors between 24 and 144 h after administration of ^{89}Zr-DFO-AC-10 (Fig. 5). Imaging data were consistent with the biodistribution data and showed that the CD30-positive tumors were discerned easily above background organs as the tissue of highest ^{89}Zr-activity accumulation. High and specific contrast was observed in the Karpas 299 model, with tumor-to-muscle ratios increasing from 18.8 at 24 h to over 51.8 at

144 h (Figs. 5 and 6A). The blocking experiment with preinjection of a 65-fold excess of the cold AC-10 antibodies before the administration of ^{89}Zr-DFO-AC-10 demonstrated the specificity of ^{89}Zr-DFO-AC-10 binding in vivo (Supplemental Fig. 2). The tumor signal was significantly reduced in the blocked mouse and was comparable to uptake in the CD30-negative A-431 tumor (Supplemental Fig. 2). Notably, the A-431 tumors were also easily distinguished on the PET/CT images but tumor-to-muscle contrast ratios were considerably lower, ranging from only 4.8 to 8.7 between 24 and 144 h after administration (Figs. 5 and 6B). ^{89}Zr-DFO-AC-10 uptake in the CD30-negative model is attributed to passive accumulation via the established mechanism of enhanced permeability and retention, and our data are consistent with other reports of ^{89}Zr-DFO-mAb radiotracers in equivalent antigen-negative tumor models (21,23,24).

After the final imaging time point (144 h), the mice were sacrificed and the radiotracer distribution was measured ex vivo (Supplemental Table 1; Supplemental Fig. 3). The data were broadly consistent with the other biodistribution data and revealed high retention of ^{89}Zr radioactivity in Karpas 299 tumors (27.0 ± 11.7 %IA/g) and lower accumulation in A-431 tumors (11.0 ± 2.0 %IA/g; $P < 0.05$). It is likely that the slightly reduced ^{89}Zr uptake in CD30-positive tumors was due to the higher administered dose (~80 μg) in the PET/CT group than in the biodistribution group (~8 μg).

Autoradiography and Histology

After the PET/CT studies, tumor and liver tissues were analyzed using digital autoradiography and histology (hematoxylin–eosin staining) (Fig. 7). The digital autoradiography data showed a higher

TABLE 1
Biodistribution of ^{89}Zr-DFO-AC-10 in Nude Mice Bearing Karpas 299 or A-431 Tumors

| Site | A-431 CD30-negative | | Karpas 299 CD30-positive | | |
	24 h ($n = 3$)	72 h ($n = 3$)	24 h ($n = 4$)	72 h ($n = 3$)	72 h, blocking* ($n = 3$)
Blood	15.83 ± 2.27	12.23 ± 2.18	9.89 ± 2.70	6.38 ± 0.46	9.49 ± 2.60
Heart	4.35 ± 1.27	3.11 ± 0.88	2.88 ± 0.36	1.71 ± 0.22	2.64 ± 0.47
Lung	6.58 ± 1.15	5.81 ± 1.07	4.60 ± 0.87	3.63 ± 0.59	4.12 ± 1.20
Liver	10.90 ± 2.10	12.61 ± 2.20	15.22 ± 1.71	11.78 ± 2.43	11.00 ± 2.32
Spleen	7.20 ± 1.40	8.21 ± 2.87	8.78 ± 2.14	8.15 ± 0.79	7.07 ± 0.46
Pancreas	1.68 ± 0.34	1.24 ± 0.30	1.05 ± 0.07	0.66 ± 0.06	0.74 ± 0.23
Stomach	1.52 ± 0.40	1.49 ± 0.20	1.09 ± 0.17	0.83 ± 0.05	0.83 ± 0.08
Small intestine	2.09 ± 0.44	1.82 ± 0.20	1.23 ± 0.20	1.12 ± 0.07	1.12 ± 0.36
Kidney	6.55 ± 1.08	6.28 ± 0.99	9.41 ± 1.78	4.22 ± 0.51	4.95 ± 0.86
Muscle	1.08 ± 0.19	0.91 ± 0.10	0.62 ± 0.06	0.49 ± 0.10	0.62 ± 0.20
Bone	2.58 ± 0.53	4.11 ± 2.73	2.12 ± 0.48	5.06 ± 0.38	2.46 ± 0.65
Tumor	8.23 ± 1.58	11.04 ± 0.40	27.21 ± 5.96	37.92 ± 8.22	22.54 ± 1.58
Tumor/blood	0.52 ± 0.12	0.90 ± 0.16	2.75 ± 0.96	5.95 ± 1.36	2.37 ± 0.67
Tumor/liver	0.76 ± 0.21	0.88 ± 0.16	1.79 ± 0.44	3.22 ± 0.96	2.05 ± 0.45
Tumor/kidney	1.14 ± 0.31	1.34 ± 0.47	2.89 ± 0.84	9.00 ± 2.23	4.56 ± 0.85
Tumor/spleen	1.26 ± 0.32	1.76 ± 0.28	3.10 ± 1.01	4.65 ± 1.10	3.19 ± 0.31
Tumor/muscle	7.63 ± 2.00	12.09 ± 1.45	43.95 ± 10.67	77.24 ± 22.92	36.21 ± 11.85
Tumor/bone	3.20 ± 0.90	2.68 ± 1.79	12.82 ± 4.03	7.49 ± 1.72	9.18 ± 2.51

*With 500-μg mAb blocking.
Data are mean %IA/g ± SD. Errors for tumor-to-tissue ratios are geometric mean of SD.
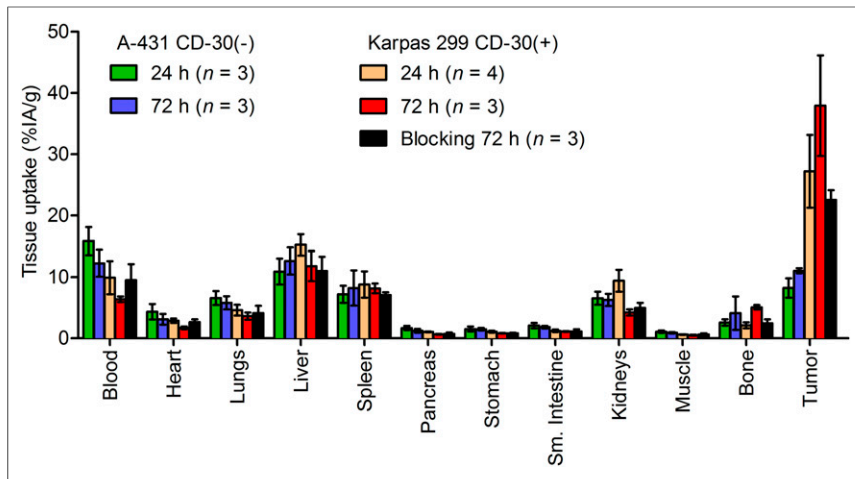
FIGURE 4. Biodistribution data showing accumulation and retention of [89]Zr-DFO-AC-10 radio-activity in various tissues vs. time in mice bearing either A-431 or Karpas 299 tumors.

accumulation of [89]Zr radioactivity in Karpas 299 tumors than in A-431 tumors or in background uptake in the liver, further confirming the specificity of [89]Zr-DFO-AC-10 binding to CD30 in vivo. The improved spatial resolution of digital autoradiography compared with PET also highlighted the intratumoral heterogeneity of [89]Zr-DFO-AC-10 distribution. Moreover, digital autoradiography demonstrated that the [89]Zr-DFO-AC-10 accumulation in CD30-negative tumor is approximately the same as in liver, whereas in CD30-positive tumors uptake is severalfold higher than in liver. These data suggest that tumor-to-liver ratios may provide a robust measure for characterizing CD30-positive versus -negative tumor expression in vivo.
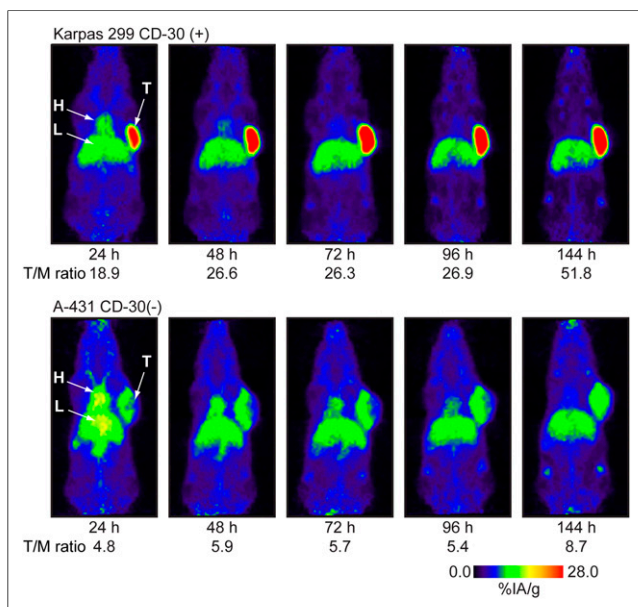

FIGURE 5. Longitudinal maximum-intensity-projection PET images showing distribution of [89]Zr-DFO-AC-10 in Karpas 299 and A-431 tumor-bearing mice 24–144 h after administration. Mean tumor-to-muscle (T/M) ratios derived from volume-of-interest analysis of PET images are given. In A-431 model, liver and tumor time–activity curves overlap. T/M = tumor-to-muscle ratio.

DISCUSSION

Brentuximab vedotin was first approved by the Food and Drug Administration in 2011 and has since received approval in more than 40 countries. ClinicalTrials.gov indicates that about 80 clinical trials are currently investigating brentuximab vedotin as a first-line, consolidation, or adjuvant therapy in patients with Hodgkin lymphoma, anaplastic large cell lymphoma, non-Hodgkin lymphoma, acute myeloid leukemia, germ cell tumors, and graft-versus-host disease. Several completed phase II trials have demonstrated the clinical efficacy of brentuximab vedotin in Hodgkin lymphoma, anaplastic large cell lymphoma, and a subset of CD30-positive non-Hodgkin lymphomas, such as diffuse large B-cell lymphomas. A trial of brentuximab vedotin in diffuse large B-cell lymphoma patients with low CD30 expression highlighted the lack of a precise quantification method for CD30 as a limiting factor in efforts to correlate target expression with clinical response (11–14). Histologic assessment of CD30 has yielded variable results. The reported data indicate that a subset of patients with lymphomas classified histologically as negative for CD30 has shown a clinical response to brentuximab vedotin treatment (11–14). This finding leads to an important clinical question pertaining to the mechanism of brentuximab vedotin activity in tumors that express low levels of CD30. The minimum threshold of CD30 expression required to render tumor sensitivity to brentuximab vedotin remains unknown.

The objective of this study was to develop a positron-emitting radiotracer as a potential companion diagnostic for use in optimizing brentuximab vedotin treatment regimens and in predicting and monitoring clinical responses. CD30 immuno-PET can potentially provide a more sensitive tool for noninvasive assessment of whole-body CD30 expression and may help to address outstanding clinical questions. As expected given the wealth of reported data on [89]Zr-DFO-mAbs, the conjugation chemistry and subsequent [89]Zr radiolabeling proceeded with high yields to give [89]Zr-DFO-AC-10. The radiotracer was found to be stable, with high immunoreactivity in vitro and in vivo. In terms of absolute tumor uptake and relative tumor-to-background tissue contrast ratios, the performance of [89]Zr-DFO-AC-10 for immuno-PET imaging of CD30-positive lesions was equivalent to the reported performance of many
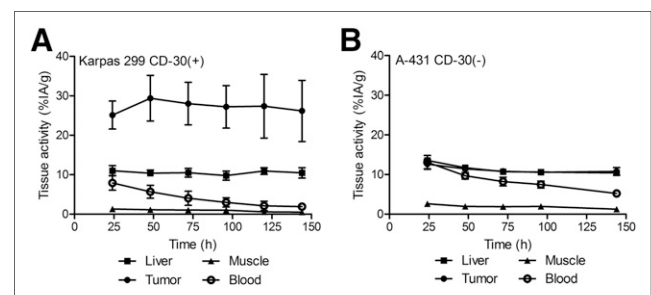
FIGURE 6. Time–activity curves derived by VOI analysis of immuno-PET/CT images showing mean %IA/g tissue uptake vs. time for [89]Zr-DFO-AC-10 radiotracer accumulation in mice bearing either Karpas 299 (A) or A-431 (B) tumors.
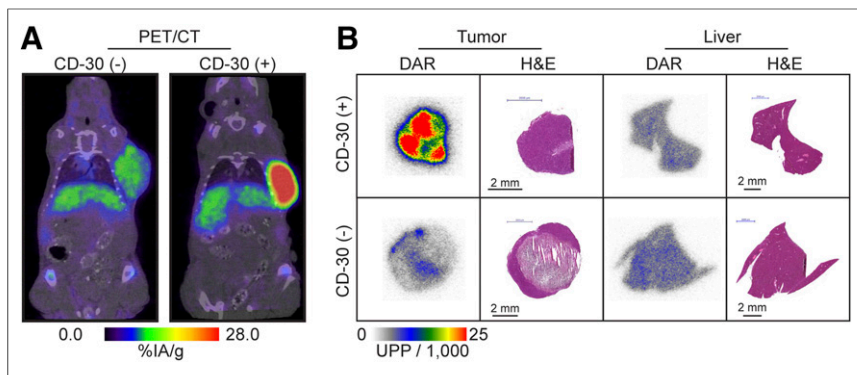
FIGURE 7. (A) PET/CT images of 2 representative mice bearing CD30-negative A-431 and CD30-positive Karpas 299 tumors at 144 h after injection. (B) Digital autoradiography and histology data showing accumulation and intratissue distribution of ^{89}Zr-DFO-AC-10 in tumor and liver for both CD30-positive and CD30-negative models. H&E = hematoxylin and eosin. DAR = digital autoradiography; UPP = • • •.

other ^{89}Zr-DFO-mAbs, including ^{89}Zr-DFO-J591 for imaging prostate-specific membrane antigen in prostate cancer (*21,25,26*), as well as ^{89}Zr-trastuzumab for imaging HER2/*neu* (*27*) and ^{89}Zr-bevacizumab imaging VEGF-A in breast cancers (*28*).

In Hodgkin lymphoma, ^{18}F-FDG PET is considered an essential tool to guide treatment intensity and modality (*29*). However, in the era of antibody-based molecular therapies, immuno-PET is becoming an increasingly attractive diagnostic tool for providing more specific information about disease distribution, staging, and treatment response. Antibody-based therapies and diagnostic agents for lymphomas have focused mostly on targeting CD20 (*30*). Well-established anti-CD20 agents include antibody-based therapy with rituximab, radioimmunotherapy with ^{90}Y-ibritumomab tiuxetan or ^{131}I-tositumomab, SPECT imaging with ^{111}In-ibritumomab tiuxetan, and PET imaging with ^{89}Zr-rituximab (*30–32*).

In contrast to reported imaging with radiolabeled anti-CD20 antibodies, ^{89}Zr-DFO-AC-10 has an advantage in that CD30 is not found in normal tissues outside the immune system and is expressed only on activated T or B cells (*2,5*). The restricted expression profile of CD30 limits nonspecific background uptake in organs such as the spleen and facilitates imaging with high contrast and specificity. A reduced background uptake in radiation-sensitive organs also suggests a future role for CD30-targeted RIT.

Overall, our data demonstrate that the novel radiotracer ^{89}Zr-DFO-AC-10 represents a promising immuno-PET agent suitable for translation to the clinic for noninvasive measurement of CD30-positive tumors.

CONCLUSION

The anti-CD30 antibody conjugate DFO-AC-10 was radiolabeled with ^{89}Zr in high radiochemical yield, purity, and specific activity. ^{89}Zr-DFO-AC-10 retained high immunoreactivity and showed specific binding to CD30 in vitro and in vivo. Immuno-PET data demonstrated that ^{89}Zr-DFO-AC-10 can be used for noninvasive imaging of CD30 expression in lymphomas and has high tumor-to-background tissue contrast. These data support ^{89}Zr-DFO-AC-10 as a promising imaging tool for selecting patients for brentuximab vedotin treatment, monitoring clinical response to optimize treatment, and minimizing brentuximab vedotin–associated toxicity.

REFERENCES

1. Kaudewitz P, Stein H, Burg G, Mason DY, Braun-Falco O. Atypical cells in lymphomatoid papulosis express the Hodgkin cell-associated antigen Ki-1. *J Invest Dermatol.* 1986;86:350–354.
2. Chiarle R, Podda A, Prolla G, Gong J, Thorbecke GJ, Inghirami G. CD30 in normal and neoplastic cells. *Clin Immunol.* 1999;90:157–164.
3. Dürkop H, Foss H-D, Eitelbach F, et al. Expression of the CD30 antigen in non-lymphoid tissues and cells. *J Pathol.* 2000;190:613–618.
4. Muta H, Podack E. CD30: from basic research to cancer therapy. *Immunol Res.* 2013;57:151–158.
5. Wahl AF, Klussman K, Thompson JD, et al. The anti-CD30 monoclonal antibody SGN-30 promotes growth arrest and DNA fragmentation in vitro and affects antitumor activity in models of Hodgkin's disease. *Cancer Res.* 2002;62:3736–3742.
6. Vaklavas C, Forero-Torres A. Safety and efficacy of brentuximab vedotin in patients with Hodgkin lymphoma or systemic anaplastic large cell lymphoma. *Ther Adv Hematol.* 2012;3:209–225.
7. van de Donk NW, Dhimolea E. Brentuximab vedotin. *MAbs.* 2012;4:458–465.
8. Pro B, Advani R, Brice P, et al. Brentuximab vedotin (SGN-35) in patients with relapsed or refractory systemic anaplastic large-cell lymphoma: results of a phase II study. *J Clin Oncol.* 2012;30:2190–2196.
9. Younes A, Gopal AK, Smith SE, et al. Results of a pivotal phase II study of brentuximab vedotin for patients with relapsed or refractory Hodgkin's lymphoma. *J Clin Oncol.* 2012;30:2183–2189.
10. Gopal AK, Chen R, Smith SE, et al. Durable remissions in a pivotal phase 2 study of brentuximab vedotin in relapsed or refractory Hodgkin lymphoma. *Blood.* 2015;125:1236–1243.
11. Moskowitz AJ. New frontiers for brentuximab vedotin for lymphomas. *Leuk Lymphoma.* 2015;56:283–284.
12. Moskowitz CH, Nademanee A, Masszi T, et al. Brentuximab vedotin as consolidation therapy after autologous stem-cell transplantation in patients with Hodgkin's lymphoma at risk of relapse or progression (AETHERA): a randomised, double-blind, placebo-controlled, phase 3 trial. *Lancet.* 2015;385:1853–1862.
13. Jacobsen ED, Sharman JP, Oki Y, et al. Brentuximab vedotin demonstrates objective responses in a phase 2 study of relapsed/refractory DLBCL with variable CD30 expression. *Blood.* 2015;125:1394–1402.
14. Blum KA. CD30: seeing is not always believing. *Blood.* 2015;125:1358–1359.
15. Zeng Z, Parekh P, Li Z, Shi ZZ, Tung CH, Zu Y. Specific and sensitive tumor imaging using biostable oligonucleotide aptamer probes. *Theranostics.* 2014;4:945–952.
16. Moss A, Gudas J, Albertson T, Whiting N, Law C-L. Preclinical microPET/CT imaging of ^{89}Zr-Df-SGN-35 in mice bearing xenografted CD30 expressing and non-expressing tumors [abstract]. *Cancer Res.* 2014;74:104.
17. Verel I, Visser GWM, Boellaard R, Stigter-van Walsum M, Snow GB, van Dongen GAMS. ^{89}Zr immuno-PET: comprehensive procedures for the production of ^{89}Zr-labeled monoclonal antibodies. *J Nucl Med.* 2003;44:1271–1281.
18. Holland JP, Sheh Y, Lewis JS. Standardized methods for the production of high specific-activity zirconium-89. *Nucl Med Biol.* 2009;36:729–739.

19. Vosjan MJWD, Perk LR, Visser GWM, et al. Conjugation and radiolabeling of monoclonal antibodies with zirconium-89 for PET imaging using the bifunctional chelate p-isothiocyanatobenzyl-desferrioxamine. *Nat Protoc.* 2010;5:739–743.

20. Verel I, Visser GWM, Boellaard R, et al. Quantitative [89]Zr immuno-PET for in vivo scouting of ^{90}Y-labeled monoclonal antibodies in xenograft-bearing nude mice. *J Nucl Med.* 2003;44:1663–1670.

21. Holland JP, Divilov V, Bander NH, Smith-Jones PM, Larson SM, Lewis JS. [89]Zr-DFO-J591 for immunoPET of prostate-specific membrane antigen expression in vivo. *J Nucl Med.* 2010;51:1293–1300.

22. Kim JS, Lee JS, Im KC, et al. Performance measurement of the microPET Focus 120 scanner. *J Nucl Med.* 2007;48:1527–1535.

23. Heneweer C, Holland JP, Divilov V, Carlin S, Lewis JS. Magnitude of enhanced permeability and retention effect in tumors with different phenotypes: [89]Zr-albumin as a model system. *J Nucl Med.* 2011;52:625–633.

24. Holland JP, Caldas-Lopes E, Divilov V, et al. Measuring the pharmacokinetic effects of a novel Hsp90 inhibitor on HER2/*neu* expression in mice using [89]Zr-DFO-trastuzumab. *PLoS One.* 2010;5:e8859.

25. Pandit-Taskar N, O'Donoghue J, Beylergil V, et al. [89]Zr-huJ591 immuno-PET imaging in patients with advanced metastatic prostate cancer. *Eur J Nucl Med Mol Imaging.* 2014;41:2093–2105.

26. Osborne JR, Green DA, Spratt DE, et al. A prospective pilot study of [89]Zr-J591/prostate specific membrane antigen positron emission tomography in men with localized prostate cancer undergoing radical prostatectomy. *J Urol.* 2014;191:1439–1445.

27. Dijkers EC, Oude Munnink TH, Kosterink JG, et al. Biodistribution of [89]Zr-trastuzumab and PET imaging of HER2-positive lesions in patients with metastatic breast cancer. *Clin Pharmacol Ther.* 2010;87:586–592.

28. Gaykema SBM, Schröder CP, Vitfell-Rasmussen J, et al. [89]Zr-trastuzumab and [89]Zr-bevacizumab PET to evaluate the effect of the HSP90 inhibitor NVP-AUY922 in metastatic breast cancer patients. *Clin Cancer Res.* 2014;20:3945–3954.

29. Gallamini A, Borra A. Role of PET in lymphoma. *Curr Treat Options Oncol.* 2014;15:248–261.

30. Suresh T, Lee LX, Joshi J, et al. New antibody approaches to lymphoma therapy. *J Hematol Oncol.* 2014;7:58.

31. Knox SJ. Levy R. CCR 20th anniversary commentary: radioactive drones for B-cell lymphoma. *Clin Cancer Res.* 2015;21:493–494.

32. Natarajan A, Habte F, Gambhir SS. Development of a novel long-lived immunoPET tracer for monitoring lymphoma therapy in a humanized transgenic mouse model. *Bioconjug Chem.* 2012;23:1221–1229.